Simulation and experimental study of Pin-Plate DC discharge plasma technique

Kadhim A. Aadim

Department of Physics, College of Science, University of Baghdad

E-mail: kadhim_adem@scbaghdad.edu.iq

Abstract

The present work intends to study of dc glow discharge were generated between pin (cathode) and a plate (anode) in Ar gas is performed using COMSOL were used to study electric field distribution along the axis of the discharge and also the distribution of electron density and electron temperature at constant pressure (P=0.03mbar) and inter electrode distance (d=4 cm) at different applied voltage for both pin cathode system and plate anode and comparison with experimental results.

Key words
COMSOL Multiphysics, pin – plate, glow discharge, simulation, plasma parameters.

Article info.
Received: Jan. 2017
Accepted: Jan. 2017
Published: Sep. 2017

دراسة عملية ومحاكاة لدبوس و صفيحة بتقنية تفريغ البلازما ذي التيار المستمر

كاظم عبدالواحد عادم

قسم الفيزياء، كلية العلوم، جامعة بغداد

الخلاصة

الهدف من البحث الحالي هو دراسة التفريغ التوهجي ذي التيار المستمر بين الدبوس (الكاثود) وصفيحة (الانود) في غاز الاركون حيث تم استخدام برنامج كومسل لدراسة توزيع المجال الكهربائي على طول محور التفريغ، وكذلك توزيع كثافة الالكترون ودرجة حرارة الالكترون عند ضغط ثابت 0.03 ملي بار والمسافة بين الاقطاب هي 4 سنتمتر عند فولتيات مسلطة مختلفة لكل من دبوس الكاثود والصفيحة الانواد ومقارنة مع النتائج التجريبية.

Introduction

The miniaturization of plasma discharges has been studied for the development of novel applications, such as plasma display panels [1, 2], materials processing [3, 4] and analytical instrumentation [5, 6]. In such applications, the plasma discharge is generally maintained at a *low pressure*. However, operating the plasma at low pressure has several drawbacks, which include expensive vacuum systems and high maintenance costs of such systems. There is growing interest in plasma processing techniques optimized for atmospheric pressure applications due to their significant advantages from an operational point of view. At atmospheric pressure, thin film deposition at very high rates is possible and cost intensive vacuum technology can be avoided. Many approaches have been proposed in recent years to overcome the problems of generating and sustaining stable, uniform and homogeneous non-thermal atmospheric pressure plasma. The types of discharges can be obtained depending on the applied voltage and the discharge current [7]. The Townsend discharge is a self-sustained discharge characterized by a low discharge current. The transition to a sub-normal glow discharge and to a normal glow discharge is marked by a decrease in the voltage and an increase in the current [8].

The advantages of the fluid models are their simplicity. Approximate solution can be satisfied by making finite element simulation using deferential equations that describe plasma energy and species transport [9].

Four kinds of species transportation in Argon plasma, Ar, Ar+, Ar*ande, were used to study plasma simulation and its transition point. Mass conservation low should be satisfied for each species separately [10], for electron we use the equation

$$\frac{\partial n_e}{\partial t} + \nabla.\Gamma_e = S_e \quad (1)$$

where n_e is the electron density, Γ_e is the electron flux, S_e is the electron creation rate.
While for another species.

$$\rho\frac{\partial(\omega_k)}{\partial t} + \rho(\boldsymbol{u}.\nabla)\omega_k = \nabla.J_k + R_k \quad (2)$$

The energy balance is solved only for electrons, assuming that ions have equal energy with neutrals.

$$\frac{\partial\varepsilon}{\partial t} + \nabla.[-\varepsilon(\mu_\varepsilon.E) - D_\varepsilon.\nabla\varepsilon] + E.\Gamma_e = S_\varepsilon \quad (3)$$

where (ε) is the internal energy of a given element with particles. Electron flux deduce from the equation

$$\Gamma_e = -n_e\mu_e E - D_e\nabla n_e \quad (4)$$

Electric field distribution were deduced using Poisson's equation

$$\epsilon_0\nabla.E = \sum_k q_k n_k \quad (5)$$

Experimental

Fig.1 shows schematic for experimental setup which used to study the dc discharge between pin-plate system with constant working pressure (0.1 mbar) argon gas using and different applied voltage to study the plasma characteristics and distribution. COMSOL Multiphysics software based to make simulation identical with experimental based on fluid model with drift-diffusion approximation.

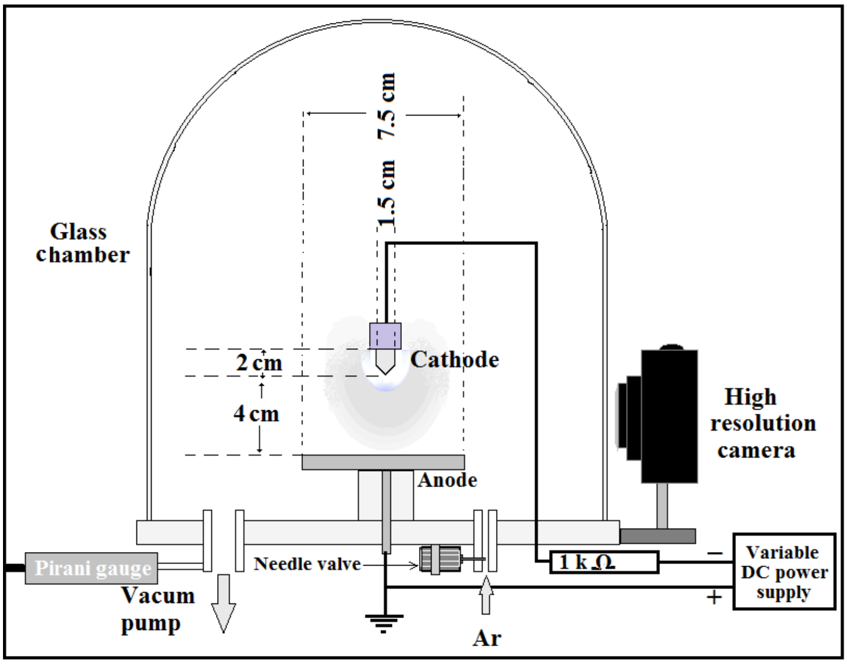

Fig. 1: Schematic for experimental setup.

Results and discussion

Fig. 2 shows the 2D axis-symmetric of our design and the mish used, and its description, for simulation which used in models (Two concentric cathodes the first is pin with radius 1.5 cm and the radius of anode is 7.5 cm with 4 cm separation between cathode and anode.

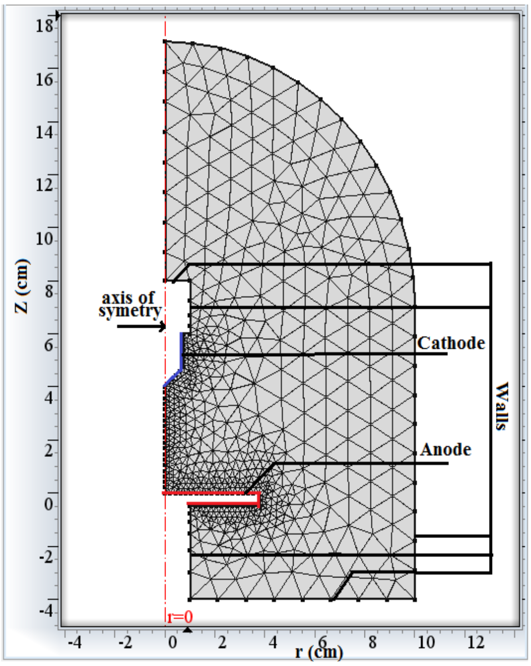

Fig. 2: Definition of 2D axial-symmetric model boundaries identical with experimental chamber.

The primary streamer discharge occurs in the vicinity of the primary streamer tip and propagates along the axial direction. Therefore, a mesh quality and size as shown in Fig. 3 is used around the needle head and along the axial symmetry line.

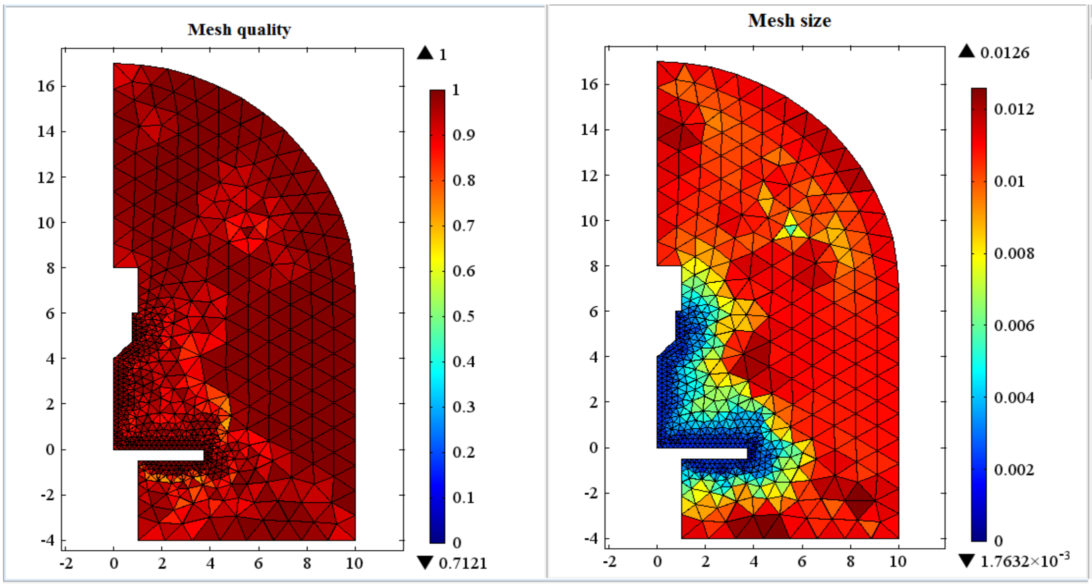

Fig.3: Experience of mesh quality and size.

Table 1 and 2 shows the used reactions in simulation which is the dominant reaction in both gas phase and surfaces reactions, respectively, and the related energy difference.

Table 1: The reactions inside the gas phase defined as follows.

No.	Reaction name	reaction	Energy (eV)
1	Electron Atom elastic collision	e+ Ar => e+ Ar	0
2	Electron impact excitation collision	e+ Ar => e+ Ar*	11.5
3	Electron impact ionization collision	e+ Ar => 2e+ Ar	15.8
4	Stepwise ionization	e+ Ar* => 2e+ Ar	4.3
5	Quenching to base state	e+Ar*=>e+Ar	-11.5
6	Penning ionization	A*+A*=>e+Ar+Ar^+	-

Table 2: The surfaces reactions used in simulation as following.

No.	reaction	Surface	Emitted Electron Energy (eV)
1	Ar^+=>Ar	Cathode	$E = 15.8 - 2\varphi$
2	Ar+=>Ar	Non cathode walls	-
3	Ar*=>Ar	All walls	-

A plot of the electric field distribution along the axis of the discharge for the base case is shown in Fig. 4. the electric field profile shows the maximum at the anode having a peak value of ~2200 V/cm with increase applied voltage from (300 – 800)V. The high electric field region indicates the edge of the cathode sheath. Within a distance of 4 cm from the cathode the electric field increases almost linearly to very high value. An electric field of ~ 600 V/cm at V=300V while electric field profile shows the maximum at V=800V. A high increase in the electric field was observed near the anode, denoting the cathode sheath.

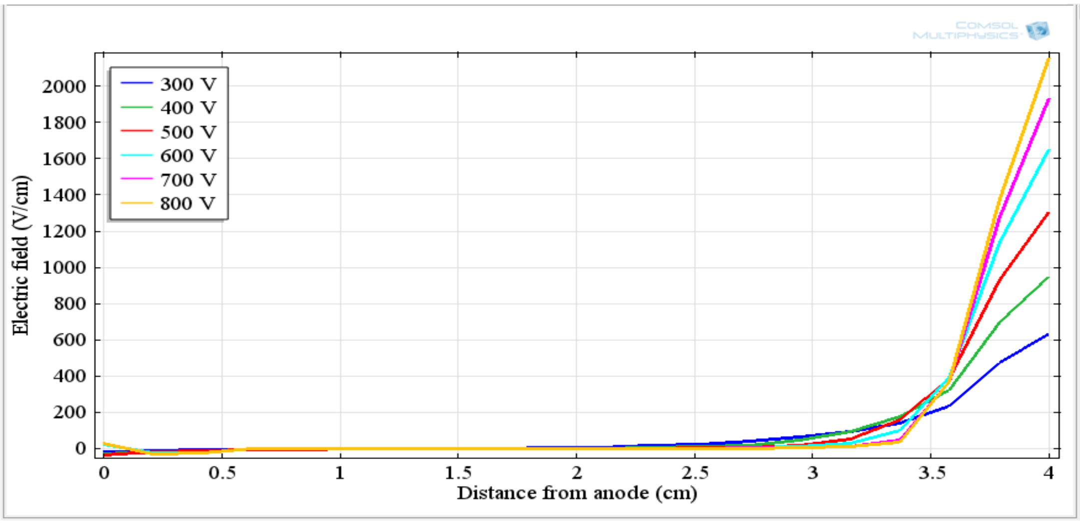

Fig. 4: Electric field profile distribution along the axial distance from anode.

Fig.5 shows the distribution of electron density at constant pressure (P=3*10^{-2}mbar) and inter electrode distance (d=4 cm) at different applied voltage for both pin cathode system and plate anode on the right. This figure indicates that the distribution being more uniformly on the region between the two electrodes when using pin cathode. From Fig. 5 note with increase the voltage difference between the two electrodes pin cathode and anode the value of the density of electron increases from (1.588×10^8 to 3.5×10^{10}) $cm^{-3}$with increasing applied voltage from (300-800)V.

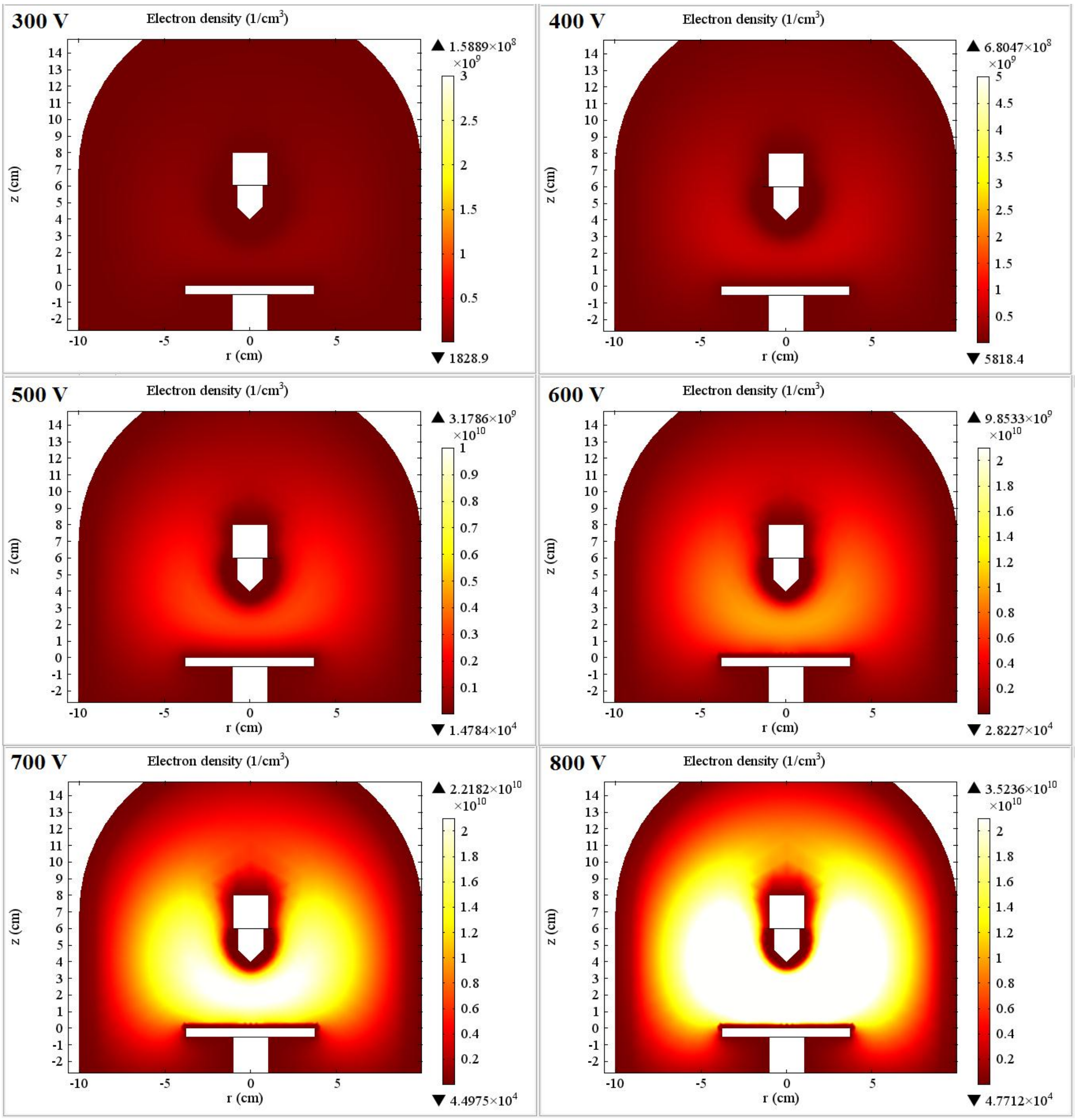

Fig. 5: The distribution of electron density with different applied voltages.

The spatial profiles of electron density extracted from the Stark width at different applied voltages are presented in Fig.6. At fixed pressure, the plasma density increases with increase discharge voltage. The electron density has maximum 3.4×10^{10} cm^{-3} at distance from anode equal to 2 cm and after that electron density decrease from (3.4×10^{10} to 0) cm^{-3} with increase distance between two electrodes from (2 to 4) cm [11].

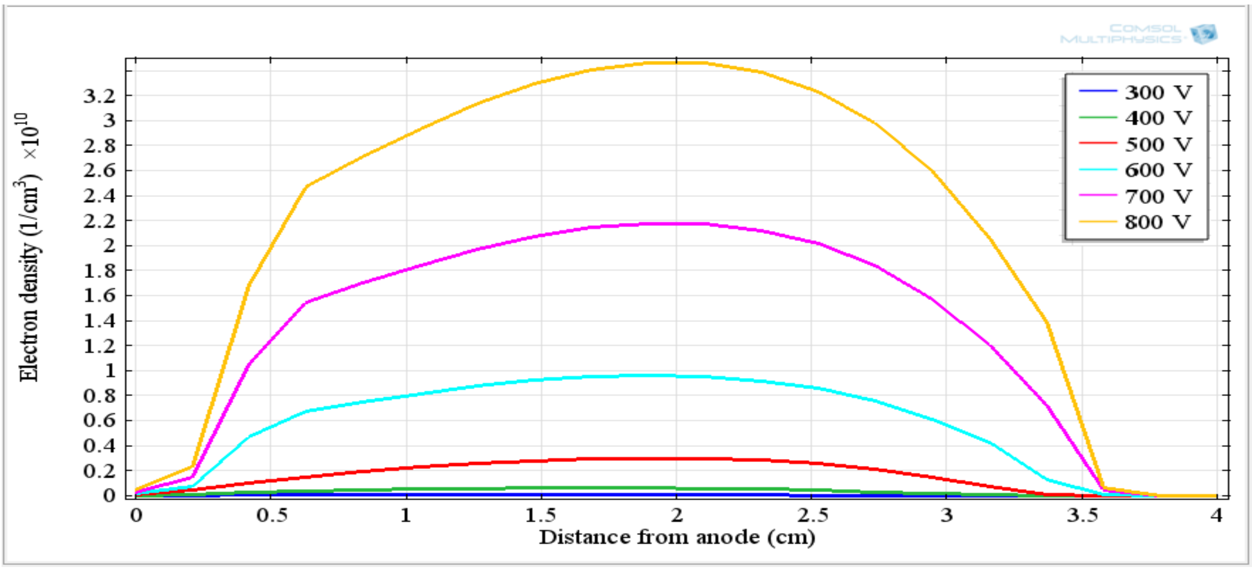

Fig. 6: Spatial profiles of electron density as a function distance from anode at different discharge voltages.

The spatial profiles of electron frequency extracted from the Stark width are presented in Fig.7. At different applied voltages, the plasma density increases with increasing discharge voltages. The electron frequency has maximum in the distance anode at 2cm, followed by a minimum. These trends are consistent with the physics of dc discharges, where most of the power dissipation occurs in a narrow layer adjacent to the anode.

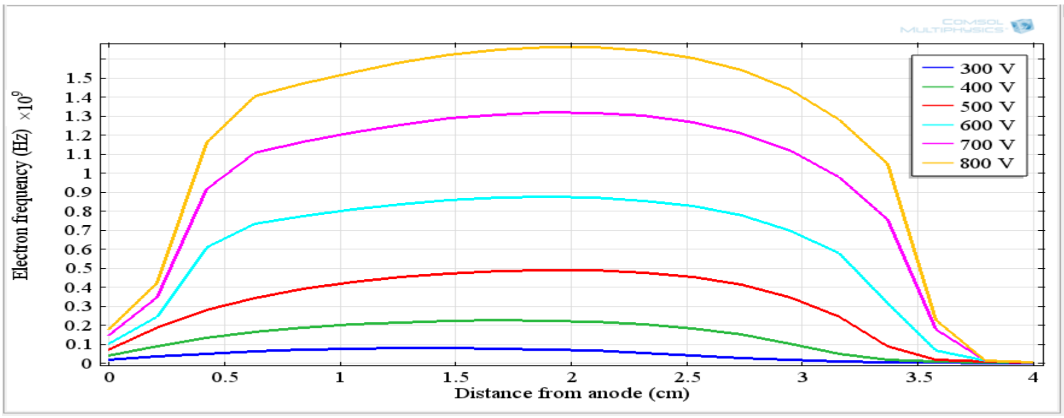

Fig. 7: Electron frequency as a function distance from anode at different discharge voltages.

Fig.8 shows the electron temperature Te as a function of a distance from anode. The electron temperature increases from 35 to 90 eV at 3.7 cm, then decreases from 36 to 14 eV at 4 cm nearly constant up to Z = 4 cm, further decreasing to 2 eV [12].

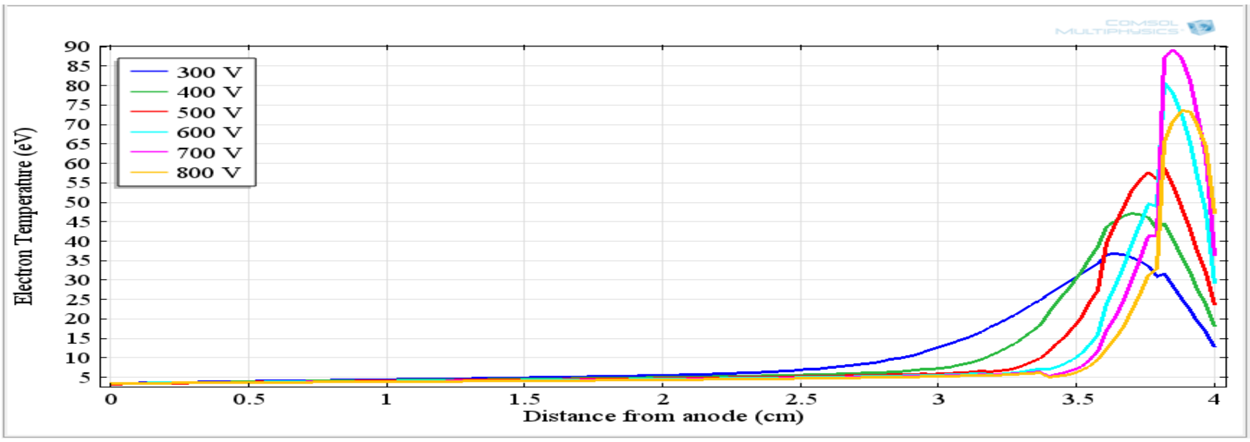

Fig. 8: Electron temperature as a function distance from anode at different discharge voltages.

Fig. 9 shows images of reaction rate with a miniature argon flow at different discharge voltages. The gap length is 4 cm. A stable glow discharge was generated at a relatively low current, as mentioned before. Increasing the applied voltages from 300 V, the visible-light intensity from the negative glow became weak and disappeared at 800 V. When the discharge voltage was increased further, a yellow light emission was observed in the negative glow region.

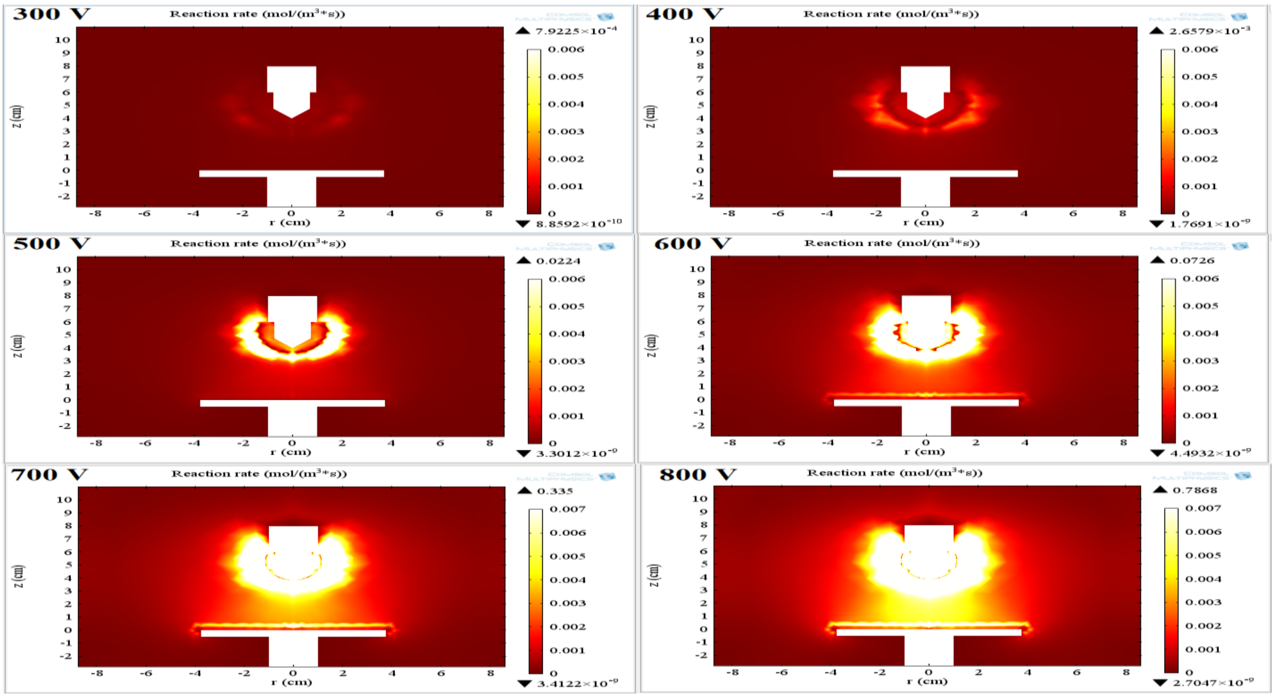

Fig. 9: Distributions of reaction rate as a function applied voltage.

Fig. 10 shows distributions of excitation rate and ionization rate as a function applied voltage; excitation rate and ionization rate are increases with increasing applied voltage. This finding suggests that the ionization efficiency of copper increase with increasing copper concentration in Ionized physical vapor deposition (IPVD). This increase in the ionization rate constant is attributed to the reduction in the electron population with energies above the ionization threshold of copper. Such depletion of the tail also reduces the ionization and excitation efficiency of argon as well. The reduction of argon optical line emission intensity with increasing dc sputtering power has been reported by Foster et al. and attributed to the Electron Energy Distribution Function (EEDF) depletion phenomena.

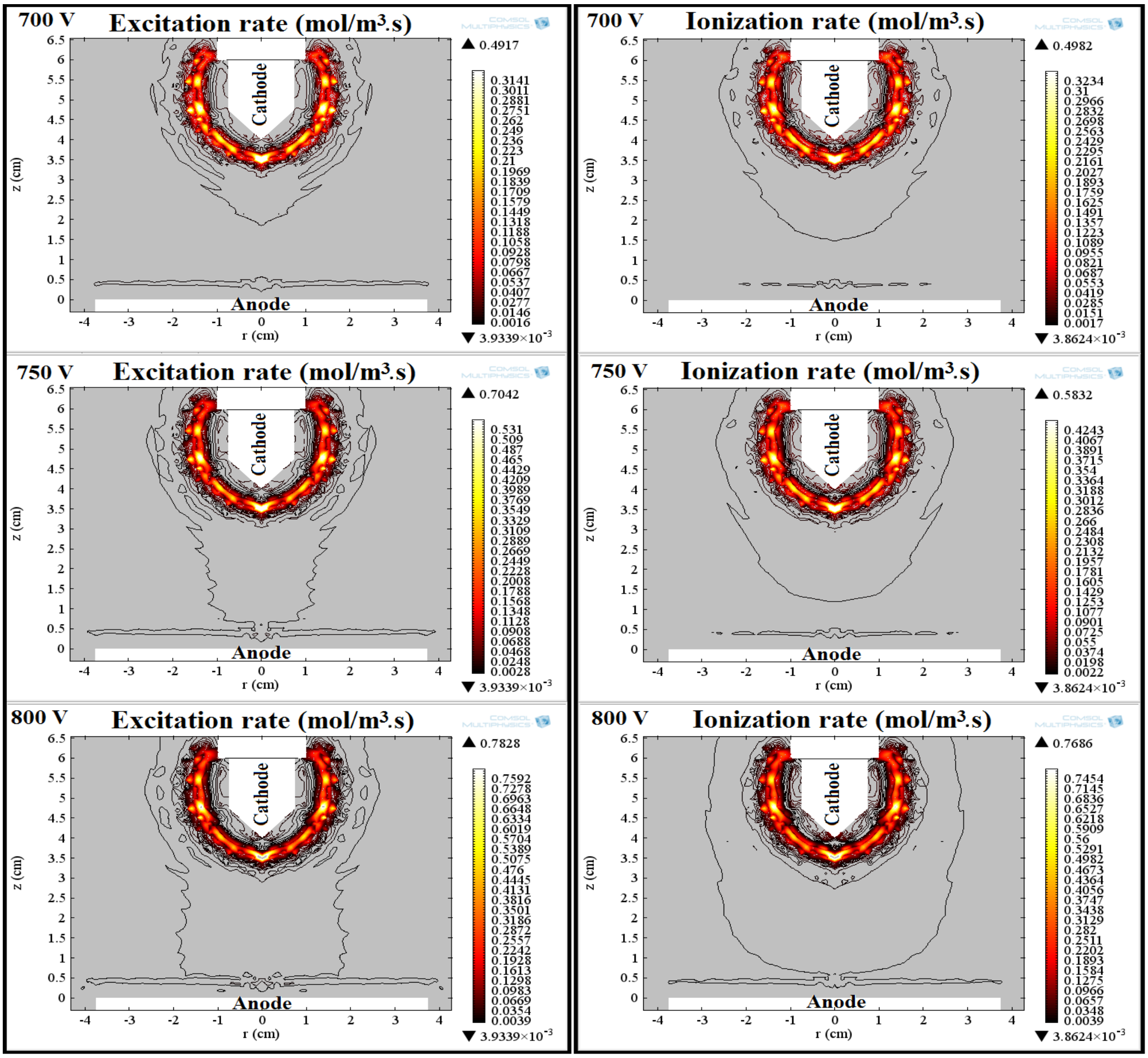

Fig.10: Distributions of excitation rate and ionization rate as a function applied voltage.

Figs. 11 and 12 shows excitation rate and ionization rate as a function distance from anode. I note from Figs.11 and 12 excitation rate and ionization rate have similar behavior but excitation rate are slightly larger from ionization rate. Excitation rates have the highest value 0.28 at 3.6 cm and increases with increasing applied voltage from (300–800) V while ionization rate has 0.24 at 3.6 cm.

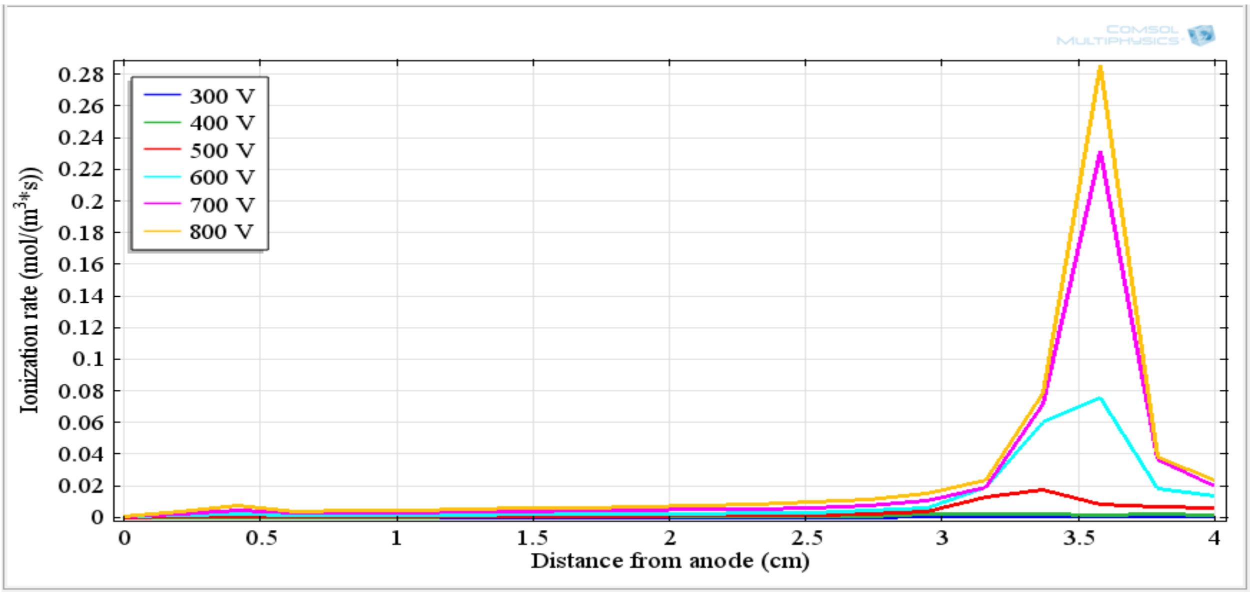

Fig. 11: Ionization rate as a function distance from anode at different discharge voltages.

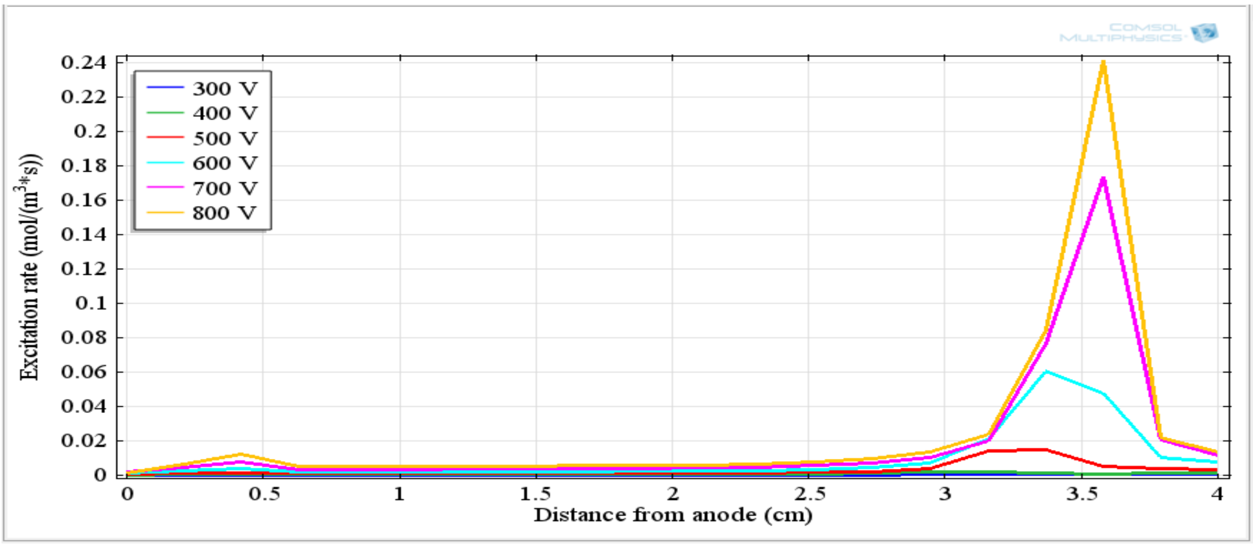

Fig. 12: Excitation rate as a function distance from anode at different discharge voltages.

Fig.13 shows Image during formation of glow discharge as a function applied voltage of reaction rate with a miniature argon flow at different discharge voltages. A glow discharge was generated at a relatively low current, as mentioned before. Increasing the applied voltages from 300 V, the visible-light intensity from the negative glow became weak and disappeared at 800 V. When the discharge voltage was increased further, a white light emission was observed in the negative glow region.

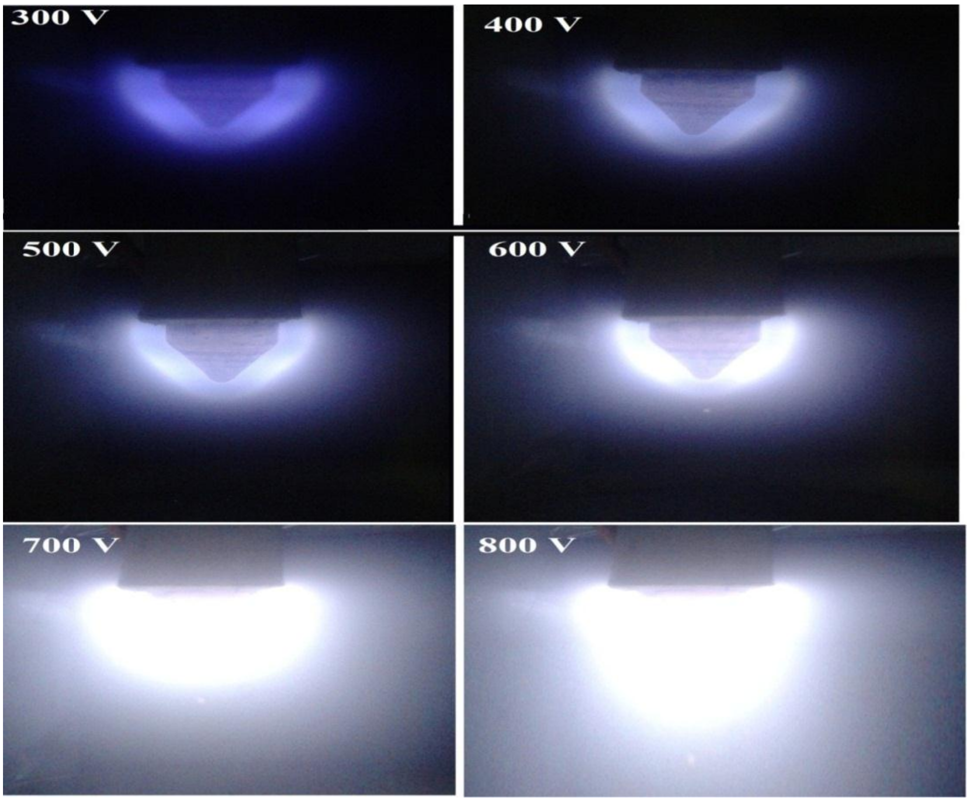

Fig.13: Image during formation of glow discharge as a function applied voltage.

Conclusions

In this paper, study electric field distribution along the axis of the discharge and also the distribution of electron density and electron temperature were generated between pin (cathode) and a plate (anode) in Ar gas is performed using COMSOL Multiphysics There was a somewhat similar, in practical and theoretical results.

References

[1] T. Callebaut, I. Kochetov, Yu Akishev, A. Napartovich, C. Leys, Plasma Sources Sci. Technol., 13 (2004) 245-250.
[2] H. Yin, J.L. He, B. Zhang, IEEE Transactions on Power Delivery, 26, 4 (2005) 2809-2820.
[3] Y. Yin, J. Messier, J. Hopwood, IEEE Trans. Plasma Sci., 27 (1999) 1516-1522
[4] L. Chen, X. Bian, L. Wang, Japanese Journal of Applied Physics, 51, 9 (2012) 61-72.
[5] O. Sakai, Y. Kishimoto, K. Tachibana, J. Phys. D: Appl. Phys., 38 (2005) 43-51.
[6] C. Labay, C. Canal, M.J. García-Celma, Plasma Chemistry and Plasma Processing, 30, 6 (2010) 327-335.
[7] Q. Wang, I. Koleva, V. Donnelly, D. Economou, J. Phys. D: Appl. Phys., 38 (2005) 1690-1697.
[8] X.B. Bian, L.C. Chen, D. Yu, IEEE Transactions on Power Delivery, 27, 3 (2012) 1693-1695.
[9] D. Staack, B. Farouk, A. Gutsol, A. Fridman, Plasma Sources Sci. Technol., 14 (2005) 700-710.
[10] Q. Wang, J. Economou, M. Donnelly, Journal of Applied Physics, 100 (2006) 233-239.
[11] Y. Kim, K. Shong, IEEE Transactions on Power Delivery, 26, 3 (2011) 1579-1584.
[12] H. Conrads and M. Schmidt, Plasma Sources Sci. Technol., 9, 4 (2000) 441-454.